Available online at www.sciencedirect.com
ScienceDirect
Robotics and Autonomous Systems 55 (2007) 72–85
Robotics and Autonomous Systems
www.elsevier.com/locate/robot

Including probabilistic target detection attributes into map representations

John Mullane, Ebi Jose, Martin D. Adams*, Wijerupage Sardha Wijesoma

School of Electrical and Electronic Engineering, Nanyang Technological University, Singapore

Received 1 October 2005; received in revised form 1 April 2006; accepted 1 June 2006
Available online 29 September 2006

Abstract

Range measuring sensors can play an extremely important role in robot navigation. All range measuring devices rely on a 'detection criterion' made in the presence of noise, to determine when the transmitted signal is considered detected and hence a range reading is obtained. In commonly used sensors, such as laser range finders and polaroid sonars, the criterion under which successful detection is assumed, is kept hidden from the user. However, 'detection decisions' on the presence of noise still take place within the sensor. This paper integrates signal detection probabilities into the map building process which provides the most accurate interpretation of such sensor data. To facilitate range detection analysis, map building with a frequency modulated continuous wave millimetre wave radar (FMCW MMWR), which is able to provide complete received power-range spectra for multiple targets down range is considered. This allows user intervention in the detection process and although not directly applicable to the commonly used 'black-box' type range sensors, provides insight as to how not only range values, but received signal strength values should be incorporated into the map building process.

This paper presents two separate methods of map building with sensors which return both range and received signal power information. The first is an algorithm which uses received signal-to-noise power to make an estimates of the range to multiple targets down range, without any signal distribution assumptions. We refer to this as feature detection based on target presence probability (TPP). In contrast to the first method, the second method does use assumptions on the statistics of the signal in target presence and absence scenarios to formulate a probabilistic likelihood detector. This allows for an increased rate of convergence to ground truth. Evidence theory is then introduced to model and update successive observations in a recursive fashion. Both methods are then compared using real MMWR data sets from indoor and outdoor experiments.

Keywords: Millimetre wave RADAR; Likelihood test; Evidence

1. Introduction

Autonomous outdoor navigation is still a very active topic of research due to the presence of unstructured objects and rough terrain in realistic situations. One of the core reasons for failure is the difficulty in the consistent detection and association of unstructured targets present in the environment. Mobile robot navigation is typically formulated as a dynamic state estimation process where predicted vehicle and target locations are fused with sensor readings. Reliable target detection from noisy sensor data is critical to the successful convergence of any such algorithm. Most methods are concerned only in the location of detected targets thus, the noise in the sensor readings are typically two-dimensional, i.e. in range and bearing. For range sensors commonly used in robot navigation such as the polaroid sonar or SICK laser, the target detection algorithm is performed internally resulting in a single (r, θ) output to the *first* signal considered detected. No other information is returned about the world along bearing angle θ, however it is typical in the case of most sensor models to assume empty space up to range r [1]. This signal may or may not correspond to a target, depending on the environmental properties, and such ambiguities can only be resolved by fusing range data from multiple vehicle locations.

In a SLAM framework, reliable target detection from the raw sensor data is of critical importance in any vehicle and map state estimation algorithm, and most SLAM methods assume targets can be consistently detected. Feature extraction is then the problem of grouping or fitting models to the detected targets so that they can readily be associated from consecutive vehicle poses. However, sensor noise in range/bearing measuring sensors is in fact three- dimensional as an added uncertainty

* Corresponding author.
E-mail addresses: john.mullane@pmail.ntu.edu.sg (J. Mullane), ebi@pmail.ntu.edu.sg (E. Jose), eadams@ntu.edu.sg (M.D. Adams), eswwijesoma@ntu.edu.sg (W.S. Wijesoma).

0921-8890/$ - see front matter © 2006 Elsevier B.V. All rights reserved.
doi:10.1016/j.robot.2006.06.010

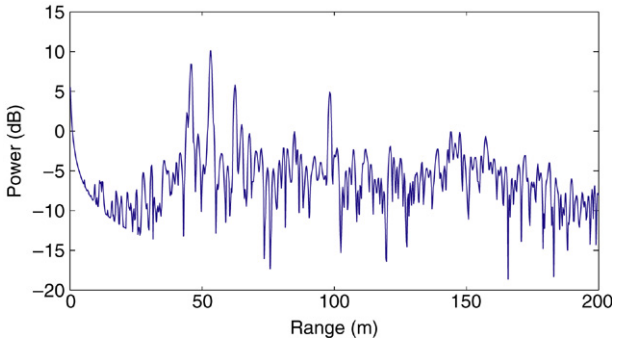

Fig. 1. Single power-range spectrum returned by the RADAR sensor.

exists in the detection process. Most navigation algorithms discard this probability and assume an ideal detector. Using this assumption, the distribution of the target co-ordinates can be conveniently modelled with probability density functions, where the probabilistic sum under the distribution is unity. That is, complete certainty that a target exists *somewhere* within that area. For occupancy based map building, the occupancy values are distributed under the constraint that the sum of the occupancy for all affected cells is unity (guaranteed from the normalization factor in Bayes rule).

Signal detectors are generally analyzed based on their receiver operation characteristics (ROC). This is simply a function of the probability of correct signal detection versus the probability of false alarm. Thus every detector has a non-unity value of signal detection and a nonzero probability of false alarm. For most sensors, users do not have access to the signal detection parameters, however this is not the case for sensors such as the Frequency Modulated Continuous Wave (FMCW) radar[1] and underwater Sonar, where the output data is a complete signal power profile along the direction of beam projection, without any signal detection being performed. At each range bin k, a power value is returned thus giving information at multiple ranges for a single bearing angle. A sample power vs. range spectrum for a fixed bearing angle is shown in Fig. 1.

These data are clearly poorly characterized and highly ambiguous as they contain correlated (in range) system noise, environmental clutter and potentially one or more targets. FMCW radar sensors are typically applied in outdoor SLAM as they can operate in hazardous environments where other sensors will fail due to its ability penetrate dust, fog, and rain [2] and harbouring their rich information can increase the speed of construction of navigational maps. Due to the often significant beamwidth of the these sensors, the wave footprint increases with range allowing for propagation passed objects thus returning range readings of multiple, partially occluded, down range targets at a single bearing angle. However, they are also very susceptible to signal noise (as can be seen in Fig. 1), target surface properties and multipath effects. The target detection problem is therefore to hypothesize whether the power at a certain range is reflected from a target, or is simply due to noise (no target). This work aims to develop a fusion framework where the confidence in target presence or absence hypotheses is recursively updated at each vehicle pose in a statistically correct manner.

This paper is organized as follows: Section 2 introduces related work in the field of radar mapping, while Section 3 gives an in-depth analysis of the signal statistics of the radar for use in the probabilistic mapping algorithms. Section 4 outlines a method of stochastic mapping which is independent of the signal statistics. An evidential mapping approach, based on a priori signal assumptions, is then developed in Section 5. Both methods are compared in Section 6 using real data acquired from outdoor tests.

2. Related work

A significant body of work exists on using Time-Of-Flight (TOF) sensors (namely laser) to perform outdoor SLAM, [3–5]. These use geometric feature extraction and scan correlation techniques to provide localization and map building. However, research into navigation using power versus range sensors is less mature.

In the underwater domain, sonars also return a power versus range vector which is difficult to interpret. In his thesis [6], Williams outlined a simple target detection technique for autonomous navigation in a coral reef environment. A constant noise power threshold is used and the maximum signal to noise ratio is chosen as the point target. Clearly this method of extraction results in a large loss of information, which is not desirable for the construction of well defined maps. Majumder attempts to overcome this loss by fitting a sum of Gaussian probability density function to the raw sensor data [7]; however, this represents a likely distribution in range of a *single point target* which is misleading as the data can contain multiple targets, leading to the association of noncorresponding points.

In field robotics, standard noise power thresholding was again used by Clark [8] using a frequency modulated continuous wave (FMCW) radar. The range and bearing covariances were then modelled and propagated through an Extended Kalman Filter framework to perform SLAM. The method was shown to work in an environment containing a small number of well separated, highly reflective beacons. The method was extended slightly in [9] where, *even bounce peculiarities* were used to extract pose invariant features. Again the environment contained reflective metallic containers. However, this conservative method of target detection limits the usefulness of the sensor since, given K range bins, only the information contained in a single bin is used. The remaining sensor data is discarded resulting in an extremely sparse map. Furthermore, as is common in most sensor models, an assumption that the noise thresholding is ideal is used, (probability of detection is one, and probability of false alarm is zero) thus there is an assumed certainty that there is a target *somewhere* at range r [10]. This sets a constraint on the occupancy distribution at that range.[2] However, in this

[1] Due to the modulating techniques, FFTs can be used to return a power value at discrete range steps. Range resolution, beamwidth, and maximum range are dependant on the particular sensor.

[2] Modelled with a pdf which integrates to unity.

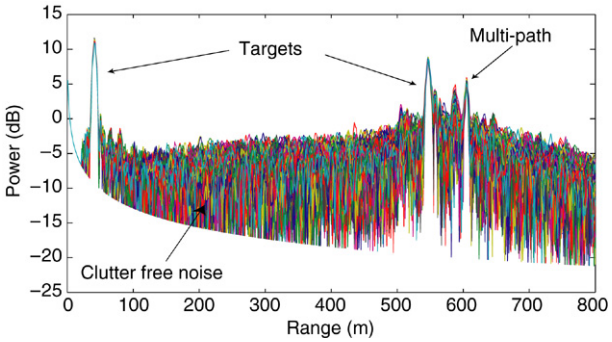

(a) Multiple range spectra plotted for the same azimuth.

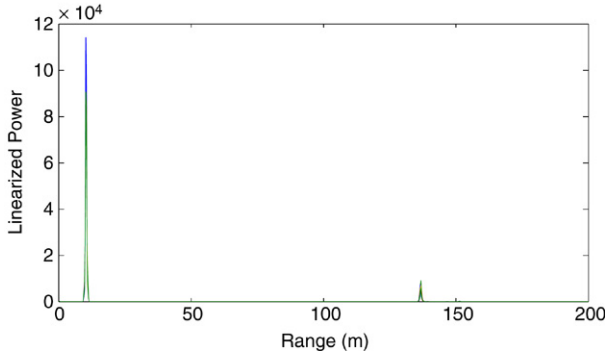

(b) Multiple range spectra plotted for the same azimuth. The power has been linearized.

Fig. 2. Multiple range spectra plotted together for the same bearing angle. Fig. 2(a) shows the full power spectra (200 m) in dB. Fig. 2(b) shows the same power spectra with linearized power values.

work, this assumption is violated due to a variable detection probability and a nonzero false alarm probability. Ignoring this fact results in the association of 'ghost' targets and the divergence of the navigation algorithm.

Stochastic detection models are preferable for power-range measuring sensors such as the FMCW radar used in this work, as the reliability of any detection algorithm is nonideal. In Foessel's paper [11], a sensor model is developed based on empirical and intuitive rules. The signal to noise ratio returned from the signal to noise likelihood is used to determine the cell occupancy probability. A Log-Odds formulation of Bayes rule is used to update the cell values in a common occupancy grid framework. Whilst this work showed promising scene modelling with the radar, it requires the use of *a priori* assigned constants to model the occupancy and its application to mobile robotics was not examined.

3. Interpretation of radar noise

MMWR noise is the unwanted power that impedes the performance of the MMWR. It is therefore the aim of this section to determine the type of noise distributions in the actual received power and range values to determine how the predicted power-range spectra can be used correctly in a robot navigation formulation. This will be needed later to justify the noise distribution assumptions used to describe the stochastic

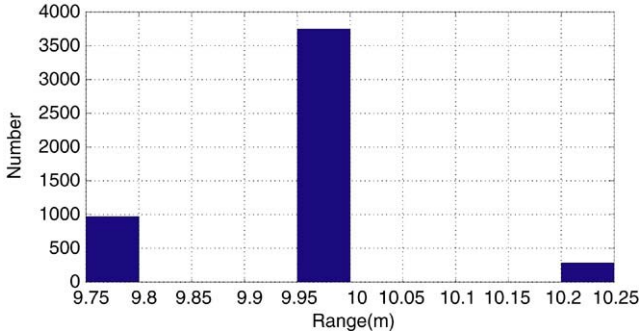

Fig. 3. Experimental histogram of noise in the range for an object at 10 m.

sensor model of Section 5. The two main noise components are thermal and phase noise.

3.1. Thermal noise

The power in the beat frequency signal (found from the FFT of this signal) is affected by the thermal noise power $a_R(t-\tau)$, which contributes to A' in:

$$v_{\text{beat}}(t,\tau) = \frac{A'}{2}\cos\left\{\left[\omega_c - \mathrm{A}_b\left(\frac{\tau}{2} - t\right)\right]\tau + \Delta\phi(t,\tau)\right\} \quad (1)$$

where $A' = [\mathrm{A}_T + a_T(t)][\mathrm{A}_R + a_R(t-\tau)]$ is the signal amplitude along with the noise affecting the amplitude. This then represents the output of the intrinsic low pass filter at the radar receiver.

3.2. Phase noise

Another source of noise which affects the range spectra is the phase noise. This is shown in Eq. (1), where a band of noise frequencies with different phase components, $\Delta\phi(t,\tau)$ affects the desired signal frequency. It is obtained from $\Delta\phi(t,\tau) = \phi(t) - \phi(t-\tau)$ and is due to the leakage of transmitted signals into the mixer [12], resulting in a spectrum of frequencies with finite bandwidth. This introduces noise into the range estimate itself. Experimental data provides insight into the phase noise distribution.

To demonstrate and estimate the phase noise effect, multiple superimposed range spectra obtained for the same radar swash plate bearing angle are plotted together as shown in Fig. 2. Fig. 2(a) shows the entire range spectrum with the returned power in dB, while Fig. 2(b) shows the same set of range spectra with the power axis linearized. Noise analysis is carried out on the range spectra with the linearized power (Fig. 2(b)). Figs. 3 and 4 show histograms obtained from two different objects (having different RCSs) at different ranges. The distributions show only the maximum power values recorded from a given target, with the radar swash plate fixed. It is apparent from Figs. 3 and 4 that the noise variance is of the order of the range resolution (25 cm).

3.3. Noise analysis during target absence and presence

The noise statistics at the radar receiver outputs during target absence and presence will now be derived. Due to the unknown

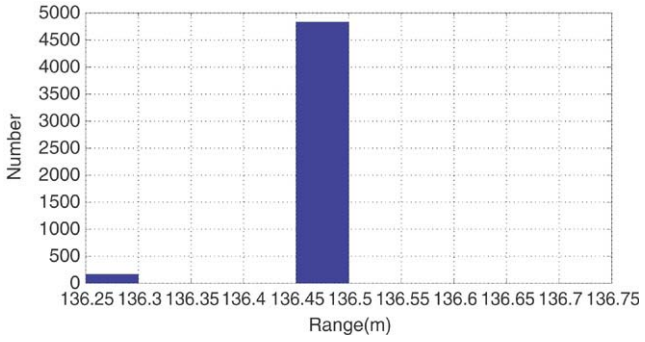

Fig. 4. Experimental histogram of range noise measured for an object at 137 m.

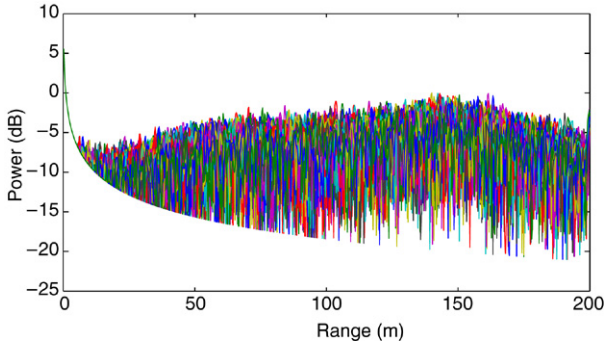

Fig. 5. Superimposed range spectra, for a constant radar swash plate bearing angle, with no targets present (swash plate pointing to the open sky).

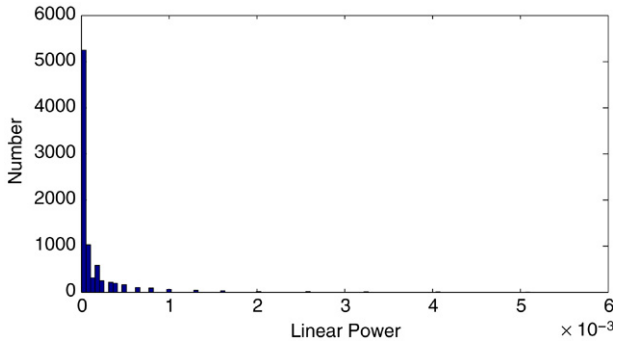

(a) Experimental estimation of the noise distribution obtained from a 25 m distance.

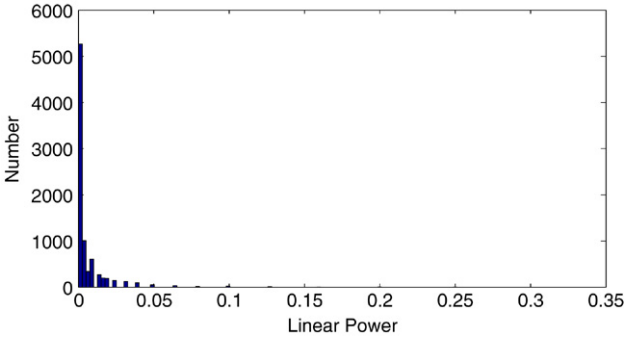

(b) Experimental estimation of the noise distribution obtained from a 100 m distance.

Fig. 6. Experimental estimation of noise power distributions, obtained at different ranges, with no targets in the environment.

nature of the exact internal components within the radar used in this work [13], an experimental determination of the noise power distributions is used here. Knowledge of the noise statistics is essential for automatic target detection methods such as Constant False Alarm Rate (CFAR) processors, that is explained further in Section 5.

3.3.1. Noise estimation in target absence

To determine the power bias and variance of the range spectra with no targets present, Fig. 5 shows superimposed range spectra, obtained at a particular radar bearing angle, recorded by pointing the radar towards the open sky. Noise analysis is carried out in the power spectra. Examination of the power distributions obtained at different ranges during target absence (derived from Fig. 5, after linearization of the spectral power values), suggests that a suitable approximation to the distributions is the exponential distribution [14]. This can be seen in Fig. 6, where power distributions at arbitrary ranges of 25 m and 100 m are shown. The exponential probability distribution function can be written as:

$$f_X(x) = \frac{1}{\mu} e^{-(x/\mu)}, \quad \forall x > 0 \tag{2}$$

where X is the random variable, the mean of the samples x is μ, which is the average power and its variance is μ^2 [14].

At a range of 25 m (Fig. 6(a)), mean value, μ for an equivalent exponential distribution[3] is 1.1×10^{-7}. For a range of 100 m (Fig. 6(b)), suitable exponential mean value have been obtained as $\mu = 4.76 \times 10^{-7}$. The two distributions obtained from different ranges indicate that the statistics are exponential throughout the range. The variance of the exponential distributions, however, are different. The interest at this stage in the analysis lies in the form of the distributions, not the variance, as knowledge of the distributions can be applied in feature detection based on CFAR processors.

3.3.2. Noise estimation in target presence

The receiver noise will also affect the signal when there is a target present. The resultant distribution is the convolution of the signal and noise distributions. A targets signal distribution is a complex function of the radar modulation type, target surface properties and radar viewing aspect. Obtaining experimental quantification of the signal distributions for the vast array of targets present in a typical outdoor navigation environment is clearly unfeasible. Therefore, the Swerling class of fluctuation models [15], commonly referred to and used in radar signal processing literature, and are also adopted in this work. With exponentially distributed noise, the joint distribution of signal and noise is assumed to be Ricean distributed. Thus, in the case of target presence, the resulting amplitude pdf is assumed to be [16]:

$$p(x|H_1) = \frac{1}{\mu} \exp\{(-x/\mu) + s\}.I_0\left(2\sqrt{\frac{sx}{\mu}}\right) \tag{3}$$

[3] This value is obtained using Matlab to fit Eq. (2) to the experimentally obtained distribution of Fig. 6(a).

where I_0 is the modified Bessel function of order zero, and s is the signal to noise ratio (SNR) sampled from the Swerling I model with mean SNR $\bar{s}$,

$$f_S(s) = \begin{cases} \frac{2s}{\bar{s}} \exp^{-s^2/\bar{s}} & \text{if } s > 0 \\ 0 \quad \text{Otherwise.} \end{cases} \tag{4}$$

4. Feature detection based on target presence probability (TPP)

For typical outdoor environments, the radar cross section of objects may be low, and buried in noise. For reducing the noise and extracting smaller signal returns along with the higher power returns, a method is now introduced which uses the probability of target presence [17] for feature detection [13]. This method is appealing compared to CFAR and constant threshold methods at ground level, as a threshold can be applied to the TPP, and any bias in the power-range spectrum does not need to be removed first, meaning that the received power values from actual targets are unaltered, leaving them range independent, assuming ideal high pass filter operation.

4.1. The target presence probability algorithm

The detection problem described here can be stated formally as a binary hypothesis testing problem [18]. Feature detection can be achieved by estimating the noise power contained in the range spectra, by averaging past spectral power values and using a smoothing parameter. This smoothing parameter is adjusted by the TPP in the range spectra. The TPP is obtained by taking the ratio between the local power value of range spectra containing noise and its minimum value. The noise power thus estimated can then be subtracted from the range spectra to give a reduced noise range spectra.

Let the power of the noisy range spectra be smoothed by a w-point window function $b(i)$ whose length is $2w + 1$

$$\check{P}(k, l) = \sum_{i=-w}^{w} b(i)\, \check{P}(k - i, l) \tag{5}$$

where $\check{P}(k, l)$ is the kth power value of lth range spectra.

Smoothing is then performed by a first order recursive averaging technique:

$$\check{P}(k, l) = \alpha_s \check{P}(k, l - 1) + (1 - \alpha_s)\check{P}(k, l) \tag{6}$$

where α_s is a weighting parameter ($0 \leq \alpha_s \leq 1$). First the minimum and temporary values of the local power are initialized to $P_{\min}(k, 0) = P_{\text{tmp}}(k, 0) = \check{P}(k, 0)$. Then a range spectrum wise comparison is performed with the present spectrum l and the previous spectrum $l - 1$.

$$P_{\min}(k, l) = \min\{P_{\min}(k, l - 1), \check{P}(k, l)\} \tag{7}$$

$$P_{\text{tmp}}(k, l) = \min\{P_{\text{tmp}}(k, l - 1), \check{P}(k, l)\}. \tag{8}$$

When a predefined number of range spectra have been recorded at the same vehicle location, and the same sensor azimuth, the temporary variable, P_{tmp} is reinitialized as:

$$P_{\min}(k, l) = \min\{P_{\text{tmp}}(k, l - 1), \check{P}(k, l)\} \tag{9}$$

$$P_{\text{tmp}}(k, l) = \check{P}(k, l). \tag{10}$$

Let the signal-to-noise power, $P_{\text{SNP}}(k, l) = \frac{\check{P}(k,l)}{P_{\min}(k,l)}$ be the ratio between the linear, local noisy power value and its derived minimum.

In the Neyman–Pearson test [19], the optimal decision (i.e. whether a target is present or absent) is made by minimizing the probability of the type II error, subject to a maximum probability of type I error as follows.

The test, based on the *likelihood ratio*, is:

$$\frac{p(P_{\text{SNP}}|H_1)}{p(P_{\text{SNP}}|H_0)} \underset{H_0}{\overset{H_1}{\gtrless}} \delta \tag{11}$$

where δ is a threshold and H_0 and H_1 designate hypothetical target absence and presence. $p(P_{\text{SNP}}|H_0)$ and $p(P_{\text{SNP}}|H_1)$ are the conditional probability density functions. The decision rule of Eq. (11) can be expressed as:

$$P_{\text{SNP}}(k, l) \underset{H_0}{\overset{H_1}{\gtrless}} \delta. \tag{12}$$

An indicator function, $I(k, l)$ is defined where, $I(k, l) = 1$ for $P_{\text{SNP}} > \delta$ and $I(k, l) = 0$ otherwise.

The estimate of the conditional TPP,[4] $\hat{p}'(k, l)$ is

$$\hat{p}'(k, l) = \alpha_p\, \hat{p}'(k, l - 1) + (1 - \alpha_p)\, I(k, l). \tag{13}$$

This TPP can be used as a target likelihood within mobile robot navigation formulations. α_p is a smoothing parameter ($0 \leq \alpha_p \leq 1$). The value of α_p is chosen in such a way that the probability of target presence in the previous range spectrum has very small correlation with the next range spectrum.

It is of interest to note that, as a consequence of the above analysis, the noise power, $\hat{\lambda}_d(k, l)$ in kth range spectrum is given by:

$$\hat{\lambda}_d(k, l) = \tilde{\alpha}_d(k, l)\hat{\lambda}_d(k, l - 1) + [(1 - \tilde{\alpha}_d(k, l))]\check{P}(k, l) \tag{14}$$

where

$$\tilde{\alpha}_d(k, l) = \alpha_d + (1 - \alpha_d)p'(k, l) \tag{15}$$

and α_d is a smoothing parameter ($0 \leq \alpha_d \leq 1$). This can be used to obtain a noise reduced spectrum, $\hat{P}_{NR}(k, l)$ using the method of power spectral subtraction [21]. In the basic spectral subtraction algorithm, the average noise power, $\hat{\lambda}_d(k, l)$ is subtracted from the noisy range spectrum. To overcome the inaccuracies in the noise power estimate, and to keep the power estimate within the working range of the radar, the following method can be used [22]:

$$\hat{P}_{NR}(k, l) = \begin{cases} \check{P}(k, l) - c \times \hat{\lambda}_d(k, l) \\ \quad \text{if } \check{P}(k, l) > c \times \hat{\lambda}_d(k, l) \\ d \times \hat{\lambda}_d(k, l) \quad \text{otherwise} \end{cases} \tag{16}$$

[4] Conditioned on the indicator function $I(k, l)$ [20].

where c, is an over-subtraction factor ($c \geq 1$) and d is spectral floor parameter ($0 < d < 1$). The values of c and d are empirically determined for obtaining an optimal noise subtraction level at all ranges and here are set to be 4 and 0.001. The performance of this algorithm will be demonstrated further in the results in Section 6.

5. Mapping based on detection evidence

Section 4 outlined a method to represent targets in a probabilistic manner, based on several recorded scans from a single robot position. However, to make a real-time tractable SLAM system, target information must be extracted from a single MMWR scan at each vehicle pose. Data returned by the MMWR is poorly characterized and can be difficult to interpret due to internal system noise and clutter masking the signal returned by the target. Furthermore, the reflected power from a target is a function of the sensors viewing aspect and fluctuates giving a nonconstant probability of detection. Therefore, SLAM using MMWR presents an extremely challenging situation of multi-target tracking with ambiguous data and variable detection probabilities. Target detection from a single realization is usually performed with likelihood tests, where the ratio of an estimated signal distribution to the noise distribution is compared to a threshold. These methods usually use some assumptions of the noise and signal distributions, whilst the moments of the distribution remain unknown and are estimated by the algorithm. Null hypothesis modelling is generally done using an exponential post-envelope noise assumption (and confirmed through experimentation in Section 3, Fig. 6) to derive a detector with constant probability of false alarm [23].

5.1. Single spectrum target detection

One of the most popular methods of detecting signals from FMCW MMWR data is through the formulation of a one-sided generalized likelihood ratio test. A single scan from pose number, n, can be written as an array of power spectra, $\mathbf{S}_n = [\mathbf{P}_{\phi_1}\mathbf{P}_{\phi_2}\cdots\mathbf{P}_{\phi_m}]^T$ where m is the number of vectors per 360° revolution. For a given spectrum, $\mathbf{P}_\phi$, its elements, $p_\phi^{1,\ldots,K}$ are modelled as K independently distributed random variables, $[X_1, X_2, \ldots, X_K]$. The sensor model must initially decide on the binary hypothesis at each range bin $k, \forall x_k = p_\phi^k, k \in \{1, 2, \ldots, K\}, \forall \mathbf{P}_\phi \in \mathbf{S}_n$. This is generally done by formulating a likelihood ratio test,

$$L(x_k) = \frac{p(x|H_1)}{p(x|H_0)} = \frac{\int p(x|\mathbf{\Psi}_1, H_1)p(\mathbf{\Psi}_1)\mathrm{d}\mathbf{\Psi}_1}{\int p(x|\mathbf{\Psi}_0, H_0)p(\mathbf{\Psi}_0)\mathrm{d}\mathbf{\Psi}_0} > T_k \qquad (17)$$

where $\mathbf{\Psi}_1$ and $\mathbf{\Psi}_0$ are the unknown parameters of the known (or assumed) distributions given target present and absent hypotheses, and x is a continuous form of the sample x_k. Note the ϕ notation is dropped as just a single power spectrum is being considered here. $L(x_k)$ is then compared against a decision threshold, T_k. The hypotheses in this case being:

$H_0 : x_k = \{\text{No Target in range bin } k\}$

$H_1 : x_k = \{\text{Target in range bin } k\}$

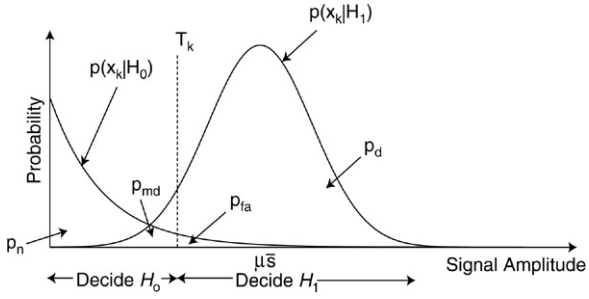

Fig. 7. Signal classification at range bin k. Here 4 probabilities are present giving the probability of correct detection of noise P_n, signal P_d, and both type I (false alarm), P_{fa} and type II (missed detection), P_{md} errors.

where x_k is a single realization of X_k. Using an IID assumption, as well as the null and alternate hypotheses signal distributions outlined previously in Section 3 we can form a likelihood test for each range bin k for a given radar power spectrum. A graphical representation of this detection problem is shown in Fig. 7.

The mean noise power μ is assumed unknown and must be locally estimated from the data in the spectrum, $\mathbf{P}_\phi$, using a moving window of width N bins.[5] From the literature [24], detectors can generally vary in their methods of generating local estimates of the noise distribution. An ordered-statistics approach has been shown to be most robust in situations of high clutter, as is commonly encountered in a field robotics environment, and is therefore adopted in this work. The decision threshold for each bin is set as normal as:

$$T_k = \tau z_k \qquad (18)$$

where, z_k is a local estimate of the average noise power μ and τ is a scaling factor to achieve a desired false alarm probability, P_{fa}, given by:

$$P_{fa} = \int_0^\infty P[x_k \geq \tau z_k | H_0] f_Z(z)\mathrm{d}z \qquad (19)$$

which can be shown to be:

$$P_{fa} = n\binom{N}{n}\frac{(n-1)!(\tau+N-n)!}{(\tau+N)!} \qquad (20)$$

where $f_Z(z)$ is the pdf of the noise estimate z_k [25]. The ordered statistic noise estimate, z_k, is chosen as $z_k = x_n$, where x_n is the nth element of the N ordered (according to amplitude) samples $[x_1, \ldots, x_N]$ in the moving window. This class of signal detector is commonly referred to a constant false alarm rate (CFAR) detector, and is favourable in this work as it provides theoretically derived values to be used in the sensor model. The output of an OS-CFAR detector with parameters $N/2 = 20$, $P_{fa} = 1 \times 10^{-6}$, $G = 2$, and $n = 3N/4$ on real MMWR data from a particular test, is shown in Fig. 8. A high RCS radar reflector was placed at 10 m, with a building at approximately 135 m. The detector correctly

[5] Typically, to account for spectral spreading, guard cells (denoted G) are included on each side of the cell under test and so the window is split into a lead and lag section.

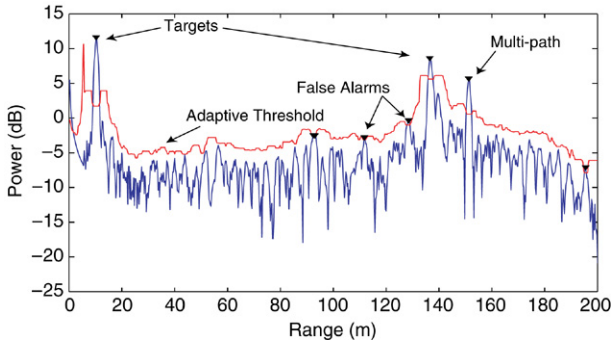

Fig. 8. OS-CFAR detector output on a single power spectrum. Numerous false alarms occur due to violation of the IID assumption.

identifies the 2 reflected target signals, with an added multipath return. However, some false alarms also occur, even in a clutter free (open air) environment. This is due to violations of the IID noise assumption, thus biased estimates of the mean noise power result in frequent false alarms.

Given the assumed signal statistics in the presence of noise and signal, as shown in Fig. 7, the four following probabilities for any CFAR process can be determined for each range bin k:

$$P_d = \int_0^\infty P[x_k \geq \tau z_k | H_1] f_Z(z) \mathrm{d}z \tag{21}$$

$$P_n = \int_0^\infty P[x_k < \tau z_k | H_0] f_Z(z) \mathrm{d}z \tag{22}$$

$$P_{md} = \int_0^\infty P[x_k < \tau z_k | H_1] f_Z(z) \mathrm{d}z \tag{23}$$

$$P_{fa} = \int_0^\infty P[x_k \geq \tau z_k | H_0] f_Z(z) \mathrm{d}z. \tag{24}$$

Clearly for a given target, P_d and P_{md} will be a function of the mean SNR, $\bar{s}$. However, given only a single realization of X_k, we make the assumption that $\bar{s} = E\{s\} \approx x_k/z_k$ (reasonable with a signal of low variance), allowing the probabilities to be readily calculated.

5.2. Detector output interpretation

The resulting set of K probability sets ($\{P_d, P_{fa}\}$ or $\{P_{md}, P_n\}$) are then put in an evidential framework for fusion and map building. They represent evidence in support of the frame of discernment:

$$\Theta = \{M_f, M_e\}$$

containing fullness and emptiness beliefs, where the subsets, denoted 2^Θ, are known as the *power set*:

$$2^\Theta = \{M_\emptyset, M_f, M_e, M_{f\cup e}\}$$

with $\emptyset$, f, e, and $f \cup e$ representing the null, full, empty and unknown sets respectively. Thus, when the observation Z_t is made the beliefs are assigned as:

$$\left.\begin{aligned} m(M_f|Z_t) &= P_d \\ m(M_e|Z_t) &= P_{fa} \\ m(M_u|Z_t) &= 1 - P_d - P_{fa} \end{aligned}\right\} \quad \text{for } x = H_1 \tag{25}$$

$$\left.\begin{aligned} m(M_f|Z_t) &= P_{md} \\ m(M_e|Z_t) &= P_n \\ m(M_u|Z_t) &= 1 - P_n - P_{md} \end{aligned}\right\} \quad \text{for } x = H_0 \tag{26}$$
$$m(M_\emptyset|Z_t) = 0 \quad \text{for } x = H_0, H_1$$

where $m(A|B)$ is the *mass distribution* on A given B. Here, $m(M_u|Z_t)$ represents the unknown or 'ignorance' evidence given sensor data at time t. Clearly in the case of hypothesis H_0 being chosen, to calculate P_{md}, a mean SNR $\bar{s}$ is required. Thus, as with the H_1 hypothesis, $\bar{s}$ is calculated using x_k, *as if it were from a target*. This then allows for an evidence of occupancy to be assigned, even though the detector declared a no target hypothesis.

To satisfy the normalizing constraint:

$$\sum_{A\subset 2^\Theta} m(A|Z_t) = 1 \tag{27}$$

we therefore set,

$$m(M_{f\cup e}|Z_t) = m(M_u|Z_t) = 1 - m(M_f|Z_t) - m(M_e|Z_t). \tag{28}$$

The resulting triplet $\{m(M_f|Z_t), m(M_e|Z_t), m(M_u|Z_t)\}$ is known as the *body of evidence*. Thus for a single power vector $\mathbf{P}_\phi$, there will be K such triplets generated. However, with the above constraint, clearly only $m(M_f|Z_t)$ and $m(M_e|Z_t)$ need to be stored to maintain a full description of the map.

5.3. Data fusion

Fusion equations for uncertain beliefs were developed by Dempster [26]. These state that given two mutually independent *bodies of evidence*, i.e. a sensor reading and a map, $m_k(A)$ and $m_m(B)$, then for any possibility C (posterior) the combined evidence provided by the two sources is given by:

$$m(C) = \frac{\sum_{A\cap B=C} m_k(A) m_m(B)}{1 - \sum_{A\cap B=\emptyset} m_k(A) m_m(B)} \tag{29}$$

where $A, B, C \subset 2^\Theta$. Thus, by discretizing the previous distributions onto a fixed grid, the beliefs on the map can be recursively updated. The numerator represents the aspects of the sensor data that confirm the map data and can be separated into the 'fullness confirmation' and 'emptiness confirmation', denoted $m(\lambda_f|Z_t)$ and $m(\lambda_e|Z_t)$. The denominator is a measure of the conflict between the new sensor data and the map data, and will be denoted $m(\kappa|Z_t)$. Thus, as with the Bayesian update, Dempsters rule of combination can fuse independent *bodies of evidence*, to recursively update the state of the map. Expanding the equation to determine the posteriors for map 'fullness', $m(M_f|Z^t)$ and 'emptiness', $m(M_e|Z^t)$, where Z^t represents all observations taken up until time t we get:

$$m(M_f|Z^t) = \frac{m(\lambda_f|Z_t)}{m(\kappa|Z_t)}$$

$$m(M_e|Z^t) = \frac{m(\lambda_e|Z_t)}{m(\kappa|Z_t)}$$

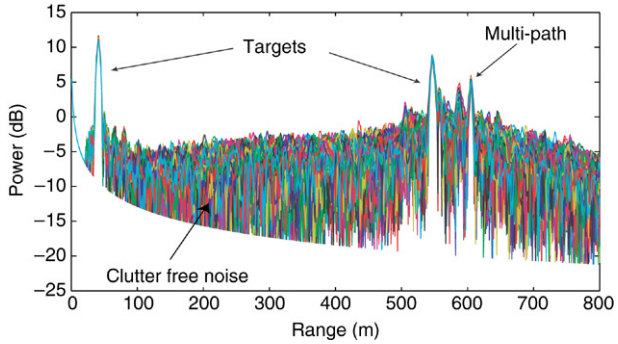

Fig. 9. Multiple fixed bearing MMWR observation.

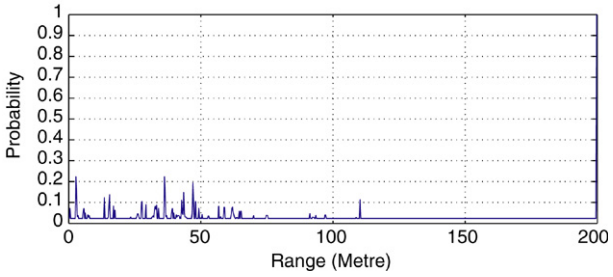

(a) Output of TPP algorithm after 30 iterations.

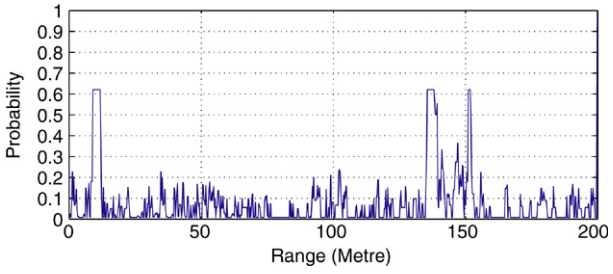

(b) Output of TPP algorithm after 40 iterations.

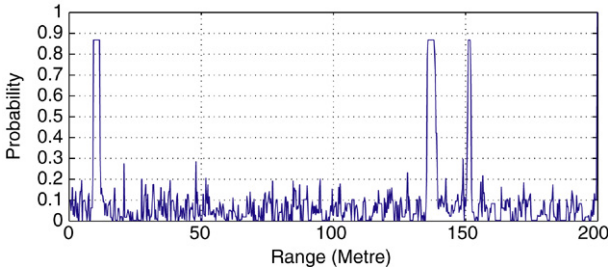

(c) Output of TPP algorithm after 50 iterations.

Fig. 10. Posterior occupancy on the map at differing iteration numbers based on the TPP algorithm.

where:

$$m(\lambda_f|Z^t) = m(M_f|Z^{t-1})m(M_f|Z_t) + m(M_u|Z^{t-1})m(M_f|Z_t) + m(M_f|Z^{t-1})m(M_u|Z_t) \quad (30)$$

$$m(\lambda_e|Z^t) = m(M_e|Z^{t-1})m(M_e|Z_t) + m(M_u|Z^{t-1})m(M_e|Z_t) + m(M_e|Z^{t-1})m(M_u|Z_t) \quad (31)$$

$$m(\kappa|Z^t) = 1 - m(M_e|Z^{t-1})m(M_f|Z_t) - m(M_f|Z^{t-1})m(M_e|Z_t). \quad (32)$$

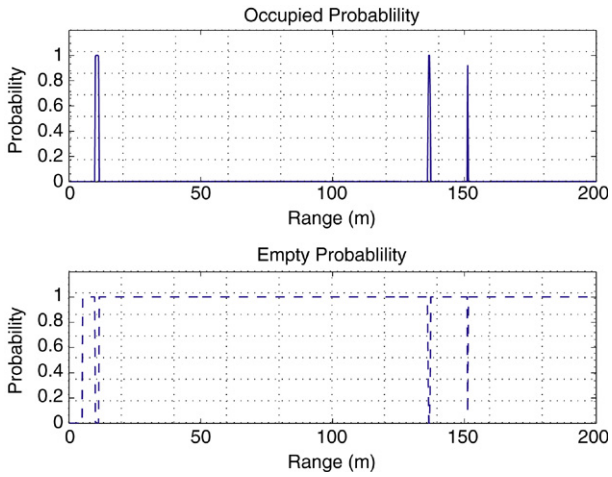

Fig. 11. Corresponding output based on the evidential sensor model after 5 iterations.

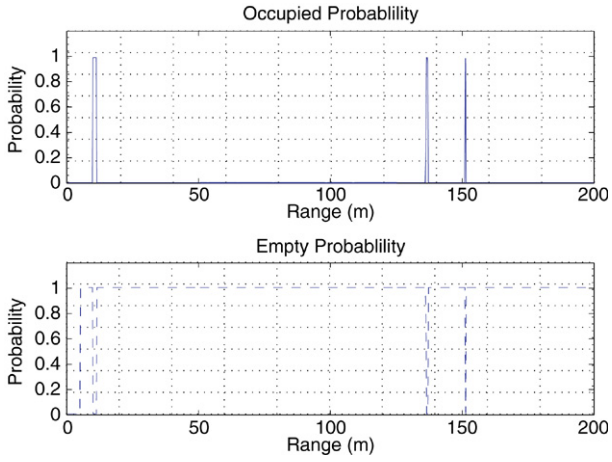

Fig. 12. Corresponding output based on the evidential sensor model after 10 iterations.

Using this formulation, both the sensor and map data are trusted equally (analogous to an equally weighted Kalman filter update). This presents a framework to identify missed detections (due to occlusion or RCS fluctuation) when the sensor indicates empty space in a previously occupied cell. This formulation also allows for unknown areas to be assigned complete ignorance.

6. Experimental results

Setting a constant threshold is clearly nonintuitive and binary CFAR techniques fail to quantify the confidence in target detection. Therefore, in this section, a comparison of the proposed TPP and evidential mapping techniques will be shown. Algorithms are run on real data collected from field experiments.

The first experiment is performed on fixed bearing power-range spectra observations obtained by disabling the rotation mechanism of the MMWR. A reflector was kept at 10 m, and multiple MMWR returns were recorded. Fig. 9 shows the raw data (i.e. multiple realizations on the underlying series

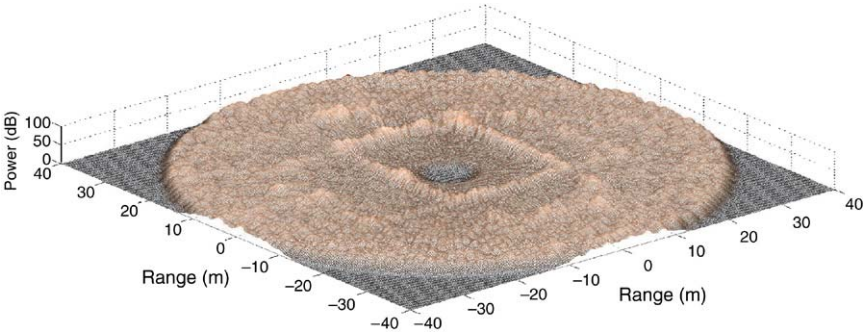

(a) Power versus range of a two-dimensional MMWR scan from an indoor environment.

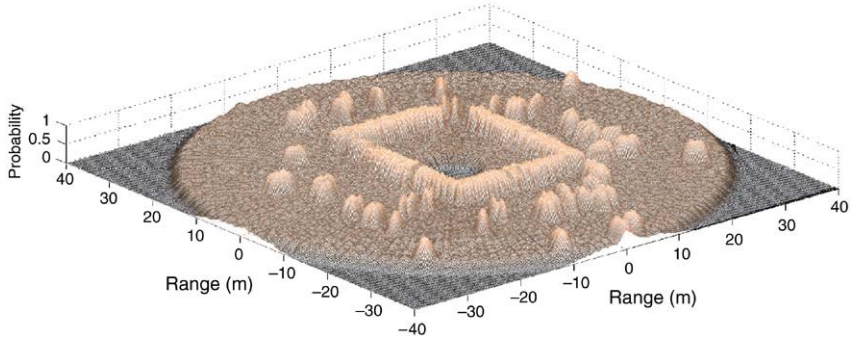

(b) TPP versus range of a two-dimensional MMWR scan in an indoor environment. The probability of the detected targets (i.e. walls) are shown in the figure.

Fig. 13. Raw MMWR data and corresponding target presence probability plots obtained from an indoor sports hall.

of (assumed independent) probability density functions). Due to the large difference in the signal variance under null and alternative hypotheses, the three reflections can be readily identified by visual inspection. Using these data, the TPP algorithm is used to detect the reflections. Due to no *a priori* assumptions being made on the signal statistics, the algorithm requires numerous samples (spectra) to converge. The output probability on target presence can be seen after 30, 40 and 50 iterations in Fig. 10.

In Fig. 9, the range bins contain three distinct reflections of differing power values, whereas the TPP plot shows the three peaks with a more uniform range width and similar probabilistic values. The second peak is from a building lying beyond the reflector, whilst the third is most likely a multi-path reflection. Such multi-path ambiguities can only be resolved by running the algorithm on a moving platform with scans from varying vehicle positions. Thus the methods presented in this paper should be interpreted as echo detectors, as the extraction of reliable environmental features requires further data processing. This result shows that, although the returned power values vary from different objects, the corresponding TPP values are similar.

The evidential model also detects the signals due to a well-tuned detector operating with a low probability of false alarm in an 'ideal' (clutter free) environment. Fig. 11 shows the output after five iterations. As the *a priori* assumptions have been made, a belief of occupancy can be obtained after just a single observation from a single spectrum. The probability of the third reflection is slightly less due to the occurrence of some missed detections. Increasing the false alarm probability Eq. (24) of the detector would reduce the missed detections at the expense a higher convergence rate. After 10 updates, the occupancy probability has approached unity for all three reflections, as can be seen from Fig. 12.

Tests are next performed on a full 360° scan from an indoor court. The purpose of the test is to see how well both algorithms extract the four court walls. The TPP-based feature detector is easier to interpret than the raw power spectra as shown in Fig. 13 where TPP plots are shown along with the corresponding raw MMWR data.

Fig. 13(a) shows the raw MMWR data and the corresponding TPP is shown in Fig. 13(b). The four walls of the stadium are clearly extracted by the proposed algorithm. The other probability values at longer range values arise due to multi-path effects. Results from the evidential model are shown in Fig. 14. Due to a minimum range of operation of the sensor (5 m), there is an 'unknown' section around the sensor origin. The occupied plot clearly shows large evidence of the four walls. False alarms are also evident due to multi-path effects and large noise contributions. Due to the strong signal generally returned by the walls (high RCS), there is little residual unknown belief after the reflection has been detected. Due to bearing encoder data acquisition problems with this particular radar, some nonuniform increases in bearing angle occur. This naturally will result in an increase in the unknown belief as seen in Fig. 14(c), as portions of the map are not scanned by the sensor.

Tests performed in an outdoor carpark are presented next. Fig. 15 shows an overview of the testing ground for

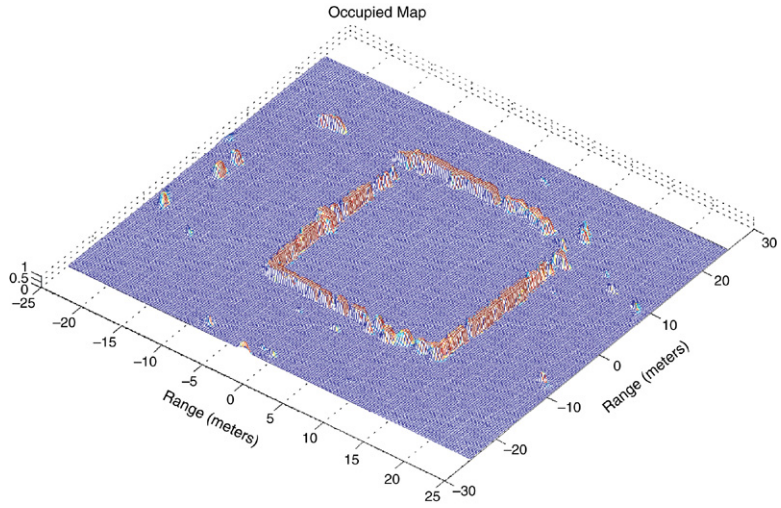

(a) Occupied map from the evidential model.

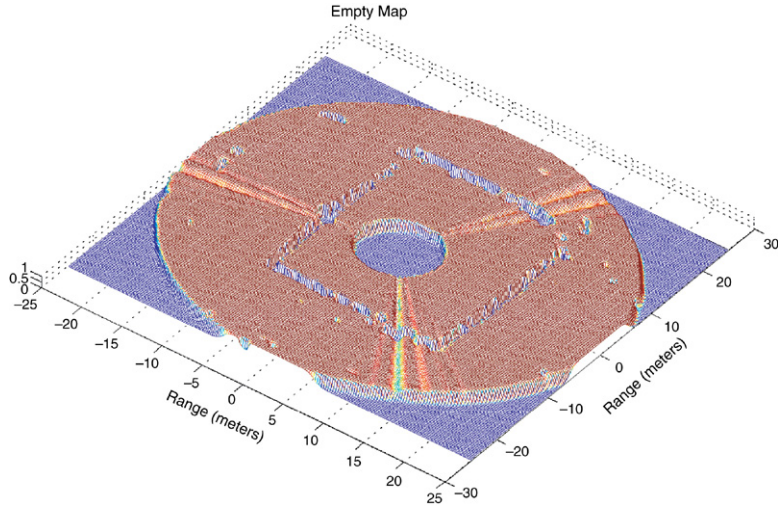

(b) Empty map from the evidential model.

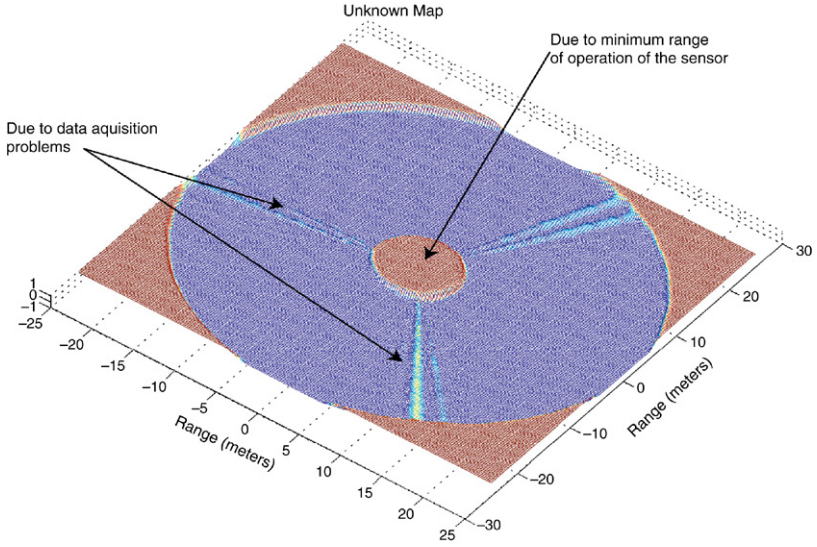

(c) Unknown map from the evidential model.

Fig. 14. Occupied, empty and unknown maps from the evidential model.

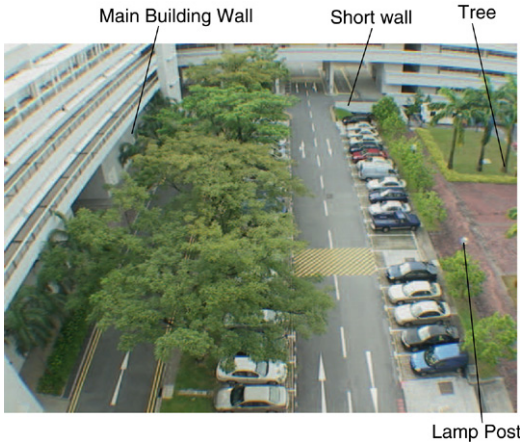

Fig. 15. Overview of testing ground (the cars were absent at the time of the scan).

comparison, as the map ground truth is difficult to obtain. Fig. 16, 17 and 18 respectively show the occupied, empty and unknown probabilities extracted from a single 360° scan from a fixed location. Objects with large RCSs return strong signals and hence leave little residual unknown probabilities, however, null hypothesis decisions, and reflections from low RCS targets leave some unknown information as can be seen from the green areas of Fig. 18.

Finally the fusion of multiple scans from a moving platform is presented. A vehicle with a mounted MMWR was driven around the carpark, recording multiple scans. Localization was performed using a scan-matching approach based on the IDC algorithm [27]. The CFAR detector selected a single point from the radar power spectrum at each bearing angle, then estimated the vehicle pose and covariance. Probabilistic occupied and empty scans were then extracted and fused in a recursive fashion. To include the noise variances in the sensor, each bin represents the peak of a bivariate Gaussian distribution in evidence. This allows for the positional covariance to be included through the standard SLAM Jacobian methods. Fig. 19 shows the occupied belief on the map from the fusion of 10 successive scans. The vehicle position is shown by black dots in the centre. Targets such as the walls, which are consistently detected, quickly approach a unity value of occupancy and can be readily identified in the figure. Fluctuating targets such as the tree and lamp post also remain in the map. This is as a result of assigning an occupied likelihood from the sensor model, when a missed detection has occurred. The evidence of multipath effects (particularly behind the wall in the region bounded by (50, 80) to (30, 0)) have been reduced to low occupancy belief, as has the region around the vehicle origin.

7. Conclusion

This paper considered the problem of signal detection and map building with range sensors for autonomous vehicles. Signal detection is rarely considered in mapping algorithms, as it is usually an internal function of the sensor and inaccessible to the user. Two methods of integrating the detection process into map building were presented and the theory was then applied to a MMWR sensor. The first method presented was the TPP algorithm which does not rely on adaptive threshold techniques, but estimates the probability of target presence based on local signal to noise power estimates, found from several successive power-range spectra. No prior assumptions need to be made on the signal statistics under target presence and absence hypothesis giving a robust detection technique.

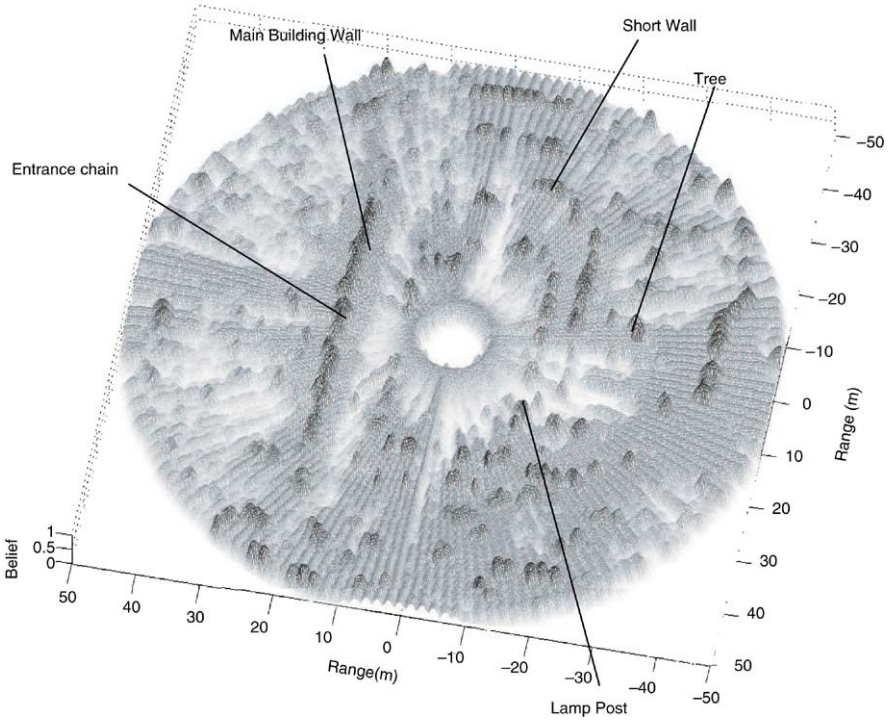

Fig. 16. Occupied map from the evidential model.

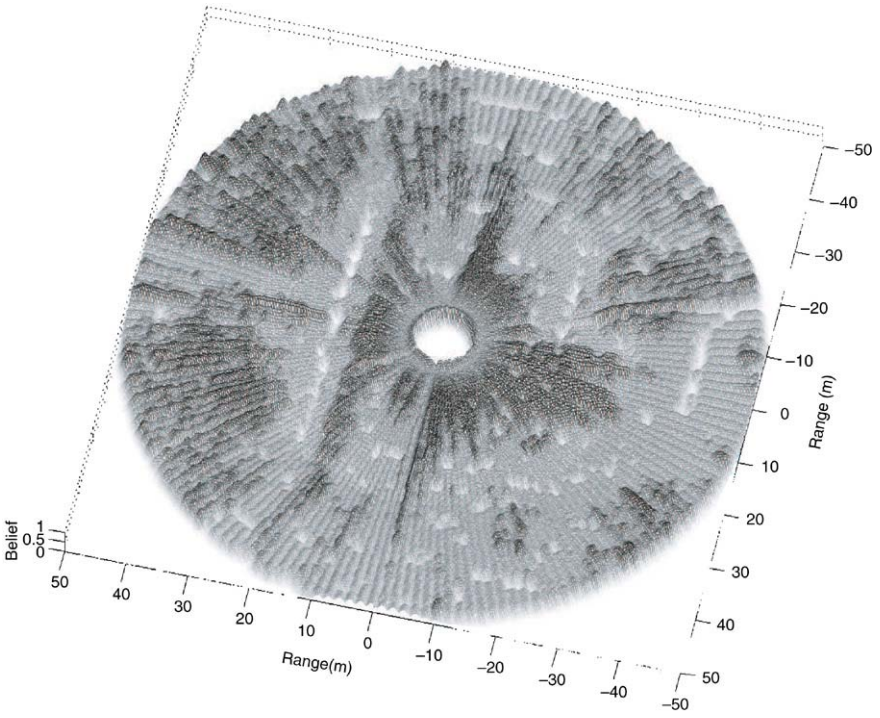

Fig. 17. Empty map from the evidential model.

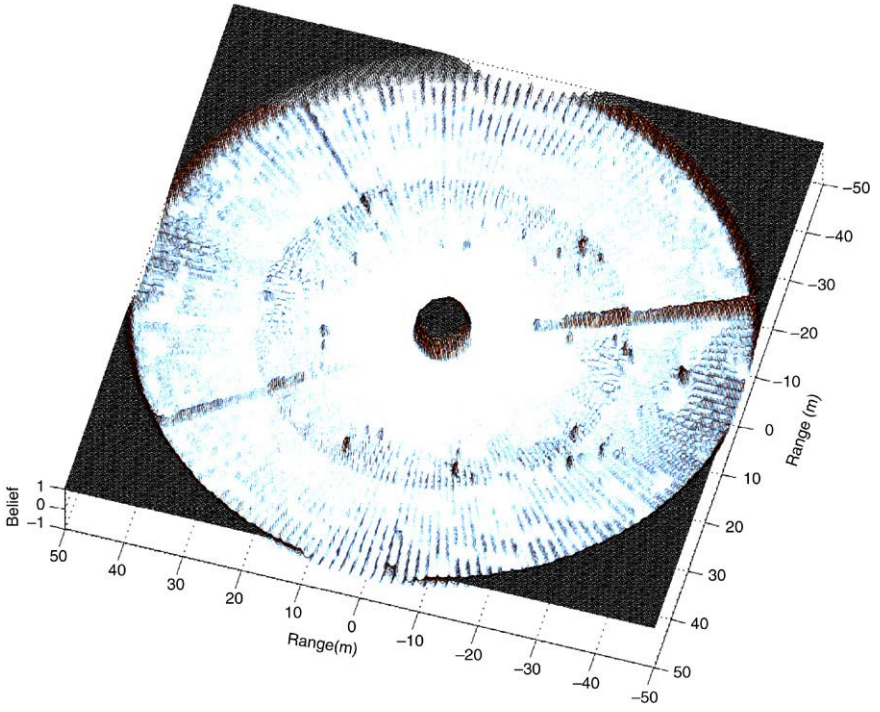

Fig. 18. Unknown map from the evidential model.

The results show that the algorithm can detect features well, however numerous iterations are required for convergence. End results however compare well with the true state.

A second model was introduced taking a different approach of using experimentally justified *a priori* assumptions on the signal statistics and using it to derive a general likelihood detector. The adaptive thresholding approach is attractive in that it can be executed given a *single* power-range spectrum. The classification probabilities were then integrated into an evidential framework for data fusion. It is argued that evidence theory is best suited for the fusion of such ambiguous data, especially with the fallacy of the cell-averaging maximum likelihood estimates in cluttered environments. This approach has attractive properties such as rigorous probabilistic

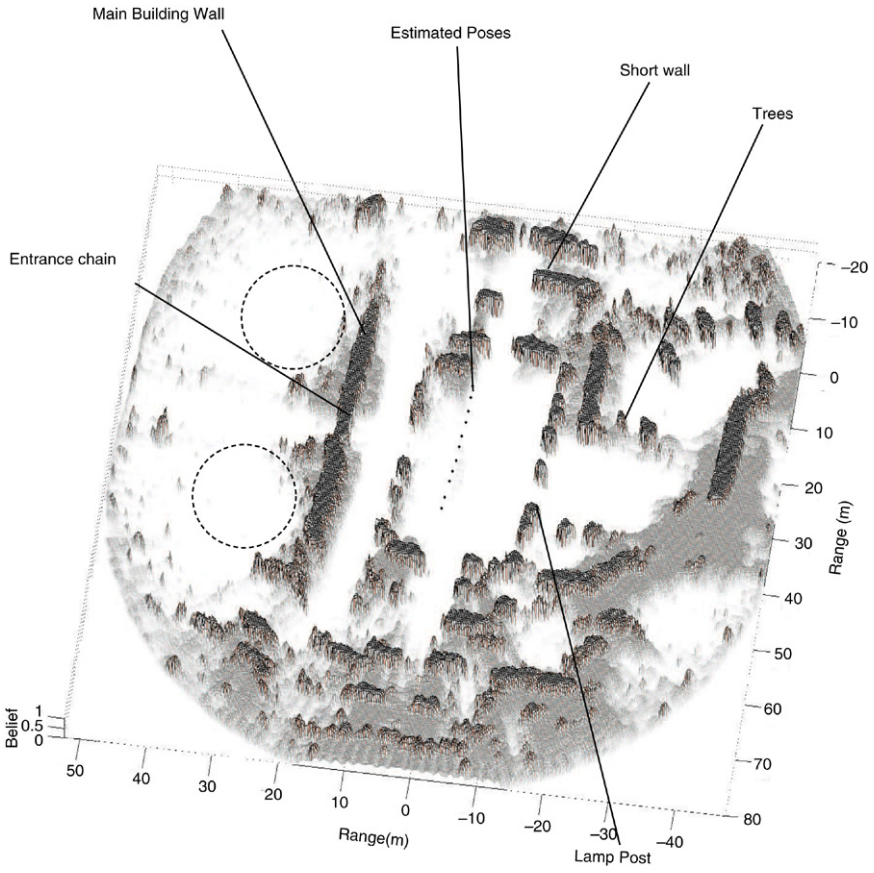

Fig. 19. Occupied plot from 10 successive scan fusions from the carpark. The estimated vehicle pose is shown by black dots along a 30 m trajectory. Dotted ellipses show regions of suppressed false detections behind the wall. Missed detection hypotheses around the vehicle location (seen in Fig. 16) have also been confirmed empty.

formulation and quantification of false alarms and missed detections. Both algorithms were tested on real MMWR data from indoor and outdoor datasets. Results were presented for the successive fusion of scans showing the merits of the second algorithm. Targets were consistently detected and their presence probability increased accordingly. Even with fluctuating RCS, the accommodation for missed detections in the model allowed for the occupancy to be maintained. False alarms were quickly eliminated as the missed detection probability for a false alarm remained low.

Occlusions and sensor model variances need to be derived and integrated into the update equations for an improved map building process. Interesting work also remains in formulating these mapping techniques into a navigation framework suitable to field robotic applications.

Acknowledgement

This work was funded under the third author's AcRF Grant, RG 10/01, Singapore.

References

[1] J.J. Leonard, H.F. Durrant-Whyte, Dynamic map building for an autonomous mobile robot, in: International Workshop on Intelligent Robots and Systems, IEEE, Ibaraki, Japan, July 1990, pp. 89–96.

[2] G. Brooker, M. Bishop, S. Scheding, Millimetre waves for robotics, in: Australian Conference for Robotics and Automation, Sidney, Australia, November 2001.

[3] J. Nieto, T. Bailey, E. Nebot, Scan-SLAM: Combining EKF-SLAM and scan correlation, in: International Conference on Field and Service Robotics (FSR), 2005.

[4] J. Guivant, E. Nebot, S. Baiker, Autonomous navigation and map building using laser range sensors in outdoor applications, Journal of Robotic Systems 17 (10) (2000) 283–565.

[5] C.-C. Wang, C. Thorpe, S. Thrun, Online simultaneous localization and mapping with detection and tracking of moving objects: Theory and results from a ground vehicle in crowded urban areas, in: IEEE International Conference on Robotics and Automation, May 2003.

[6] S. Williams, Efficient Solutions to autonomous mapping and navigation problems, Ph.D. Thesis, Australian Centre for Field Robotics, University of Sydney, 2001.

[7] S. Majumder, Sensor fusion and feature based navigation for subsea robots, Ph.D. Thesis, The University of Sydney, August 2001.

[8] S. Clark, H. Durrant-Whyte, Autonomous land navigation using millimetre wave radar, in: International Conference on Robotics and Automation, ICRA, IEEE, Leuven, Belgium, May 1998, pp. 3697–3702.

[9] S. Clark, G. Dissanayake, Simultaneous localisation and map building using millimetre wave radar to extract natural features, in: International Conference on Robotics and Automation, ICRA, IEEE, Detroit, Michigan, May 1999, pp. 1316–1321.

[10] H. Moravec, A.E. Elfes, High resolution maps from wide angle sonar, in: Proceedings of the 1985 IEEE International Conference on Robotics and Automation, March 1985, pp. 116–121.

[11] A. Foessel, J. Bares, W.R.L. Whittaker, Three-dimensional map building with MMW RADAR, in: Proceedings of the 3rd International Conference on Field and Service Robotics, Helsinki, Finland, June 2001, Yleisjljenns - Painnoprssi.

[12] M.E. Adamski, K.S. Kulpa, M. Nalecz, A. Wojtkiewicz, Phase noise in two-dimensional spectrum of video signal in fmcw homodyne radar, in: 13th International Conference on Microwaves, Radar and Wireless Communications, MIKON-2000, vol. 2, 2000, pp. 645–648.
[13] E. Jose, M.D. Adams, Millimetre wave radar spectra simulation and interpretation for outdoor SLAM, in: International Conference on Robotics and Automation, ICRA, New Orleans, USA, April 2004.
[14] D.C. Montgomery, G.C. Runger, Applied Statistics and Probability for Engineers, second ed., John Wiley and Sons, Inc, 1999.
[15] P. Swerling, Probability of detection for fluctuating targets, IRE Transactions on Information Theory 6 (1960) 269–308.
[16] H. Rohling, R. Mende, OS CFAR performance in a 77 GHz radar sensor for car applications, in: CIE International Conference of Radar, October 1996, pp. 109–114.
[17] I. Cohen, B. Berdugo, Noise estimation by minima controlled recursive averaging for robust speech enhancement, IEEE Signal Processing Letters 9 (1) (2002).
[18] H.L. Van Trees, Detection, Estimation and Modulation Theory—Part I, Wiley, New York, 1968.
[19] T. Kirubarajan, Y. Bar-Shalom, Multisensor-Multitarget Statistics in Data Fusion Handbook, CRC Press, Boca Raton, 2001.
[20] R.M. Gray, L.D. Davisson, Introduction to Statistical Signal Processing, Cambridge University Press, December, 2004.
[21] S.F. Boll, Supression of acoustic noise in speech using spectral subtraction, IEEE Transactions on Acoustic, Speech and Signal Processing 27 (2) (1979) 113–120.
[22] M. Berouti, R. Schwartz, J. Makhoul, Enhancement of speech corrupted by acoustic noise, in: Proceedings of the IEEE ICASSP'79, 1979, pp. 208–211.
[23] P.P. Gandhi, S.A. Kassam, Analysis of cfar processors in nonhomogeneous background, IEEE Transactions on Aerospace and Electronic Systems 4 (24) (1988) 427–445.
[24] H. Rohling, Some radar topics: Waveform design, range (cfar) and target recognition, Il Ciocco, Italy, July 2005.
[25] H. Rohling, Radar cfar thresholding in clutter and multiple target situations, IEEE Transactions on Aerospace and Electronic Systems 19 (1983) 608–621.
[26] G. Shafer, A Mathematical Theory of Evidence, Princeton University Press, New Jersey, 1976.
[27] E. Milios, F. Lu, Robot pose estimation in unknown environments by matching 2d range scans, Journal of Intelligent and Robotic Systems 18 (3) (1997) 249–275.

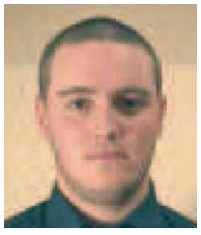

John Mullane is a Ph.D. student at the School of Electrical and Electronic Engineering, Nanyang Technological University (NTU), Singapore. He obtained his B.E. degree in electrical and electronic engineering from University College Cork (UCC), Cork, Ireland in 2002. During his degree he worked in the RF circuit design industry in Boston, USA, and was involved in the design and layout of RF and low noise amplifiers. His current research interests include radar signal processing, ground-based radar data fusion, and outdoor mobile robotics.

Ebi Jose is a Ph.D. student at the School of Electrical and Electronic Engineering, Nanyang Technological University (NTU), Singapore. He obtained his B.Tech. degree in instrumentation from Cochin University of Science and Technology, Kerala, India in 2002. During his degree he worked in the semiconductor testing industry where he designed and developed equipment for the nondestructive testing of semiconductor devices. His current research interests include MMWR sensor perception, radar signal processing, online feature detection and autonomous navigation of land vehicles.

Martin D. Adams obtained his first degree in Engineering Science at the University of Oxford, UK, in 1988 and continued to study for a D.Phil. at the Robotics Research Group, University of Oxford,which he received in 1992. He continued his research in autonomous robot navigation as a project leader and part time lecturer at the Institute of Robotics, Swiss Federal Institute of Technology (ETH), Zurich, Switzerland. He was employed as a guest professor and taught control theory from 1994 to 1995. From 1996 to 2000, he served as a senior research scientist in robotics and control, in the field of semiconductor assembly automation, at the European Semiconductor Equipment Centre (ESEC), Switzerland.

He is currently Associate Professor in the School of Electrical and Electronic Engineering, NTU, Singapore. He serves as associate editor of a leading international journal and was the coordinator of the SLAM workshop at the 2005 IEEE International Conference on Intelligent Robots and Systems. He is the principle investigator of many research projects and his research interests include autonomous vehicle navigation and robotics, focusing on scene interpretation with LADAR/RADAR and vision, integration of inertial navigation sensors (INS) and GPS and Simultaneous Localisation and Map Building (SLAM).

Wijerupage Sardha Wijesoma (M'99) received the B.Sc. Engineering Hons. degree in electronics and telecommunication engineering from the University of Moratuwa, Sri Lanka, in 1983, and the Ph.D. degree in robotics from Cambridge University, Cambridge, UK, in 1990. He is an Associate Professor of the school of Electrical and Electronic Engineering, Nanyang Technological University (NTU), Singapore. He is also the Programme Director for Mobile Robotics of the Centre for Intelligent Machines, NTU. He was previously the Head of the Department of Computer Science and Engineering, University of Moratuwa, Sri Lanka. His research interests are in autonomous land and underwater vehicles, with emphasis on problems related to navigation and perception. Dr Wijesoma is a member of the British Computer Society and a Chartered Information Systems Engineer (C. Eng.) of the Engineering Council of the UK. He is a founding committee member of the IEEE Systems, Man, and Cybernetics Society Chapter, Singapore, Committee Member of IEEE Oceanic Engineering Society Chapter, Singapore.